SAR by kinetics for drug discovery in protein misfolding diseases

Sean Chia[a,1], Johnny Habchi[a,1], Thomas C. T. Michaels[a,b,1], Samuel I. A. Cohen[a], Sara Linse[c], Christopher M. Dobson[a], Tuomas P. J. Knowles[a,d], and Michele Vendruscolo[a,2]

[a]Centre for Misfolding Diseases, Department of Chemistry, University of Cambridge, Cambridge CB2 1EW, United Kingdom; [b]Paulson School for Engineering and Applied Sciences, Harvard University, Cambridge, MA 02138; [c]Department of Biochemistry & Structural Biology, Center for Molecular Protein Science, Lund University, 221 00 Lund, Sweden; and [d]Department of Physics, Cavendish Laboratory, Cambridge CB3 0HE, United Kingdom

Edited by Michael L. Klein, Temple University, Philadelphia, PA, and approved August 14, 2018 (received for review May 7, 2018)

To develop effective therapeutic strategies for protein misfolding diseases, a promising route is to identify compounds that inhibit the formation of protein oligomers. To achieve this goal, we report a structure–activity relationship (SAR) approach based on chemical kinetics to estimate quantitatively how small molecules modify the reactive flux toward oligomers. We use this estimate to derive chemical rules in the case of the amyloid beta peptide (Aβ), which we then exploit to optimize starting compounds to curtail Aβ oligomer formation. We demonstrate this approach by converting an inactive rhodanine compound into an effective inhibitor of Aβ oligomer formation by generating chemical derivatives in a systematic manner. These results provide an initial demonstration of the potential of drug discovery strategies based on targeting directly the production of protein oligomers.

Alzheimer's disease | amyloid beta peptide | protein misfolding | protein aggregation | chemical kinetics

Alzheimer's disease (AD) is a leading cause of death in the aging populations of the modern world, and its prevention or treatment is one of the greatest medical challenges of our generation (1). This devastating disease, along with ∼50 other protein misfolding disorders, is associated with the formation and proliferation of intractable amyloid aggregates formed by a range of human peptides and proteins. (2–6). In the case of AD, the aggregation of Aβ is widely considered to be the source of a cascade of events leading to this disorder (2–6). This view has led, in the last two decades, to a dramatic increase in the efforts aimed at developing effective drugs to prevent or slow down the self-assembly process of Aβ (4, 7–10). A major objective in the field, therefore, is to identify reliable and effective means for the rational identification and systematic optimization of lead compounds in drug discovery strategies (5, 11–13). Ideal targets for developing new readouts are the intermediate species formed during Aβ aggregation, which can be highly cytotoxic (14, 15). The heterogeneous and transient nature of these species, however, requires the development of novel approaches to define their characteristics and to identify their populations and their origins (16, 17).

Here we address this issue using a chemical kinetics approach, as recent advances in this strategy have enabled an increasingly detailed analysis of the molecular events leading to protein aggregation at a microscopic level (18, 19). For example, in the case of Aβ42, the highly aggregation-prone 42-residue isoform of Aβ, the combination of a highly reproducible and quantitative kinetic experimental assay and an analytical solution to the master equation describing the aggregation process has allowed macroscopic measurements to be related to the microscopic steps in the aggregation process at a highly detailed level (19). These kinetics measurements have led to the determination of the complex reaction network responsible for generating different aggregated forms of Aβ42, and to the quantitative measurement of the reactive fluxes associated with the various microscopic events during the overall aggregation process (19).

The identification of the kinetically dominant steps in the generation of Aβ42 aggregates is particularly relevant, as these events constitute promising targets for the development of treatments to combat AD. Previous studies have shown that a molecular chaperone, a Brichos domain, can suppress surface-catalyzed secondary nucleation of Aβ42 as well as of the Aβ42-induced impairment of hippocampal gamma oscillations (20). Furthermore, small molecules have been found to inhibit the primary nucleation events in the aggregation of Aβ42, and shown to suppress significantly the cytotoxic effects associated with the aggregation of Aβ42 in vitro, in neuronal cells and in a *Caenorhabditis elegans* model of AD (13, 21). This type of information is of great importance for drug discovery because it allows the establishment of links between a targeted microscopic step in the aggregation process and the resulting effect on the generation of toxic intermediates (12, 22).

In the present study, we have made a major step forward in the use of chemical kinetics for drug discovery for AD by introducing a readout based on Aβ oligomer levels derived from measured reaction rate constants. In this method, the effectiveness of a compound is measured by its effects on the generation of Aβ oligomers. As these oligomers are particularly cytotoxic, this approach is directly aimed at enabling the development of compounds capable of reducing the neuronal death associated with Aβ aggregation.

We implement this strategy in the framework of the well-established structure–activity relationship (SAR) approach in

Significance

Protein oligomers are increasingly recognized as the most cytotoxic forms of protein aggregates. It has been very challenging, however, to target these oligomers with therapeutic compounds, because of their dynamic and transient nature. To overcome this problem, we present here a "structure–kinetic-activity relationship" (SKAR) approach, which enables the discovery and systematic optimization of compounds that reduce the number of oligomers produced during an aggregation reaction. We illustrate this strategy for the amyloid beta peptide (Aβ), which is closely associated with Alzheimer's disease, by developing a rhodanine compound capable of dramatically reducing the production of Aβ oligomers. As this strategy is general, it can be applied to oligomers of any protein.

Author contributions: S.C., J.H., T.C.T.M., S.I.A.C., S.L., C.M.D., T.P.J.K., and M.V. designed research; S.C. and J.H. performed research; S.C., J.H., T.C.T.M., S.I.A.C., S.L., C.M.D., T.P.J.K., and M.V. contributed new reagents/analytic tools; S.C., J.H., T.C.T.M., S.I.A.C., S.L., C.M.D., T.P.J.K., and M.V. analyzed data; and S.C., J.H., T.C.T.M., S.I.A.C., S.L., C.M.D., T.P.J.K., and M.V. wrote the paper.

The authors declare no conflict of interest.

This article is a PNAS Direct Submission.

[1]S.C., J.H., and T.C.T.M. contributed equally to this work.

[2]To whom correspondence should be addressed. Email: mv245@cam.ac.uk.

This article contains supporting information online at www.pnas.org/lookup/suppl/doi:10.1073/pnas.1807884115/-/DCSupplemental.

drug discovery. In SAR, through highly reproducible quantification methods, such as half-maximal inhibitory concentration (IC_{50}) values, one can determine the degree of inhibition of a given molecule and hence relate its chemical structure to its potency. However, this concept is not readily applicable to address diseases associated with protein aggregation, due to the lack of robust preclinical primary assays. In the current study, we aim to bridge this gap by describing a strategy for the rational design and systematic optimization of drug-like small molecules against the oligomers produced on pathway to aggregation.

The present strategy, which we refer to as "structure–kinetic-activity relationship" (SKAR), is based on the quantitative correlation between the changes in the chemical features of a compound and the corresponding variations in the reactive flux toward oligomers and overall fibril formation. We show that the SKAR strategy allows the rational identification and optimization of lead compounds designed to combat AD, and that this application has led to an increase in the potency of small molecules by several fold, as well as enabling the generation of potent derivatives from an inactive parent compound. Given the generality of the phenomenon leading to protein misfolding diseases, these data suggest strongly that SKAR is a powerful tool that can be used systematically for the development of drugs against protein misfolding diseases in general.

Results

The SKAR Strategy. This strategy consists of a chemical kinetics platform applied to drug discovery against misfolding diseases to (*i*) correlate the chemical structure of a candidate therapeutic molecule with its ability to inhibit oligomer production during the aggregation of a target protein and (*ii*) optimize this ability by rationally changing the chemical properties of the molecule to generate more-effective inhibitors that reduce oligomer production even further (Fig. 1). In this approach, from a specific scaffold of a parent molecule, individual chemical modifications are introduced while keeping the remainder of the molecule unchanged, thus generating a pool of derivatives with similar chemical characteristics, except for the specific groups that have been altered in this manner (Fig. 1*A*).

The next step in the procedure is the measurement of the macroscopic aggregation kinetics of the protein in the presence of the derivatives through a ThT-based assay (23) (Fig. 1*B*). In this way, any change in the half-time of aggregation ($t_{1/2}$) induced by a given small molecule can be obtained (Fig. 1*C*). By carrying out such experiments in the presence of a range of concentrations of the small molecule, it is also possible to estimate the changes in the reactive flux toward oligomers from global fitting to the experimental curves (24) (*Materials and Methods*, Fig. 1*C*, and *SI Appendix*, Eq. **S2**). To carry out a quantitative analysis, we have adopted three specific parameters associated with the

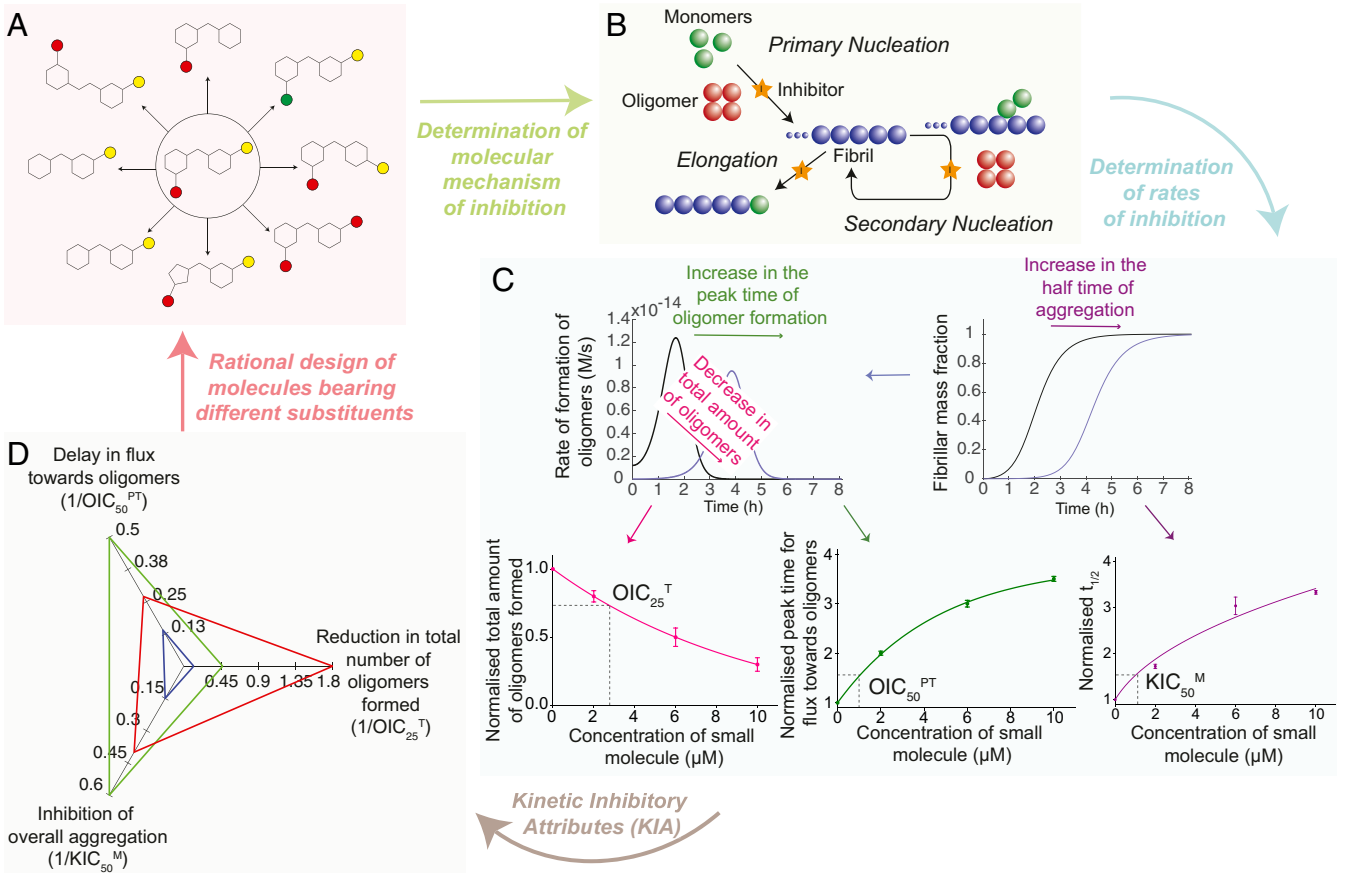

Fig. 1. Schematic illustration of the SKAR strategy. An in vitro kinetic analysis is used to determine the effects of a pool of derivatives from a particular molecular scaffold on the aggregation of the target aggregating protein, here Aβ42. (*A*) A pool of molecule derivatives from a particular scaffold is first collected for the study. (*B*) These molecules are then tested in vitro to determine quantitatively their effects on the different microscopic steps of the Aβ42 aggregation. (*C*) Kinetic rates related to the production of oligomers in the presence of small molecules are then extracted from the kinetic profiles, and three parameters are estimated: (*i*) OIC_{50}^{PT} (green), which is associated with a delay in the flux toward oligomers; (*ii*) OIC_{25}^{T} (pink), which is associated with a reduction in the total number of oligomers generated; and (*iii*) the macroscopic parameter KIC_{50}^{M} (purple), which is associated with the macroscopic kinetic inhibition. (*D*) Using these three parameters, the KIA fingerprint is constructed (*SI Appendix*, Table S1) to compare the different molecules and select the most potent ones. SKAR can be applied in an iterative manner to identify more potent derivatives or explore different chemical scaffolds.

aggregation kinetics, which, taken together, correspond to the IC_{50} parameter commonly used in SAR. These parameters are (*i*) the concentration of a given molecule that results in a 50% increase in the $t_{1/2}$ value of the overall aggregation reaction, denoted here as KIC_{50}^{M}, where KIC refers to "kinetic inhibitory concentration" and M refers to "macroscopic"; (*ii*) the concentration of the small molecule that results in a 50% increase in the time to reach the peak value of the generation of oligomers, denoted here as OIC_{50}^{PT}, where OIC refers to "oligomer inhibitory concentration" and PT refers to "peak time"; and (*iii*) the concentration of the small molecule that results in a 25% decrease in the total number of oligomers formed during the reaction, denoted here as OIC_{25}^{T}, where T refers to "total concentration of oligomers" (*Materials and Methods* and Fig. 1*C*).

More generally, we note that SKAR is an approach that enables the quantitative determination of the extent to which a small molecule affects the reactive flux toward any target species of interest in an aggregation reaction, and then to enhance its efficacy. The use of appropriate parameters corresponding to the SAR IC_{50} enables the determination of the potency of any compound for a specific process, for example, to reduce the peak levels of oligomer formation, or to change the total quantity of fibrils generated over time.

While KIC_{50}^{M} reflects a macroscopic effect obtained directly from the overall aggregation process, OIC_{50}^{PT} and OIC_{25}^{T} reflect the changes induced by a small molecule on specific microscopic steps in the aggregation process. Taking these three parameters together, a unique fingerprint of a molecule is generated, which is denoted here as the "kinetic inhibitory attributes" (KIA) fingerprint. The KIA fingerprint reflects the potency of a compound in inhibiting the specific steps in the aggregation process responsible for the production of the majority of oligomeric species (Fig. 1*D* and *SI Appendix*, Table S1). Thus, the KIA fingerprint allows a comparison to be made between the potencies of different compounds in reducing the number of potentially toxic species generated during aggregation. For instance, a KIA fingerprint such as the one shown in green in Fig. 1 reflects a molecule whose major effect is on primary events in aggregation, hence generating a delay in the formation of oligomeric species, i.e., leading to an increase in the time taken to reach the peak of the reactive oligomer flux (21). On the other hand, a KIA fingerprint such as that shown in red indicates a molecule that inhibits the surface-catalyzed secondary nucleation, thus resulting in both a delay in the reactive flux toward oligomers and a reduction in the total number of oligomers formed (20). In addition, it is evident from their KIA fingerprints that both molecules show a greater potency in all three attributes compared with that of the molecule with the blue KIA fingerprint.

The detailed understanding offered by the KIA fingerprint is a key element guiding the optimization and search for drugs with the potential to combat AD, because it allows a relationship to be established between the chemical modifications introduced into a parent molecule and the resulting changes in the rate and quantity of the production of Aβ42 oligomers. With such a relationship, this process can then be used iteratively to systematically and rationally design and optimize small molecules with increasing potency. Here we show two examples where SKAR against Aβ42 has been applied to two different parent scaffolds leading to (*i*) an understanding of the chemical properties that are responsible for an inhibitory effect on Aβ42 aggregation and (*ii*) an exploitation of this understanding to increase the potency of a different parent molecule.

Lead Compound Optimization Against Aβ42 Oligomer Production. We illustrate the SKAR strategy by its application to bexarotene, a small molecule found to inhibit strongly the nucleation of Aβ42 aggregation (21). Ten molecules bearing different substituents of R_1 (the polar moiety), R_2 (the linker group), and R_3 (the apolar moiety) were considered for this study, some of which (E, H, and G) had two of these features modified concomitantly. We generated the KIA fingerprints for all 10 molecules and compared their effects on the different microscopic steps in the process of Aβ42 aggregation (13, 24) (Fig. 2 and *SI Appendix*, Fig. S1).

The aggregation kinetics of a 2 μM Aβ42 sample were monitored in the absence and presence of each compound at concentrations ranging from 2 μM to 10 μM [datasets for bexarotene, molecules D through H, and J, were obtained from a previous

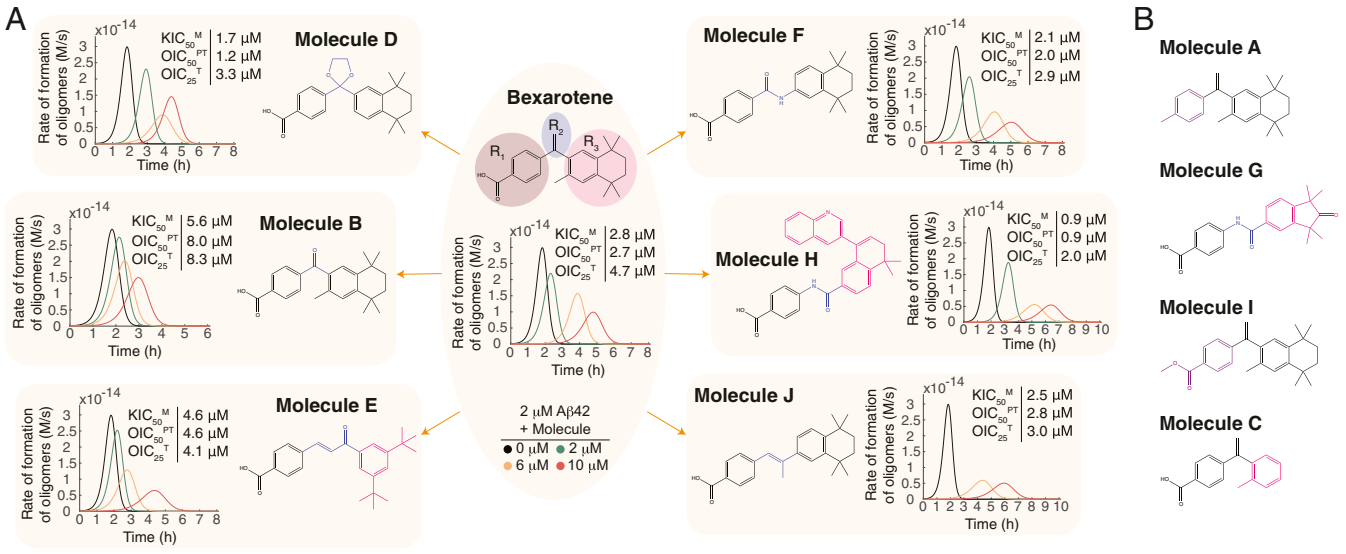

Fig. 2. Derivation of the SKAR rules from the analysis of the bexarotene scaffold. The 10 derivatives (A through J) of bexarotene used in this study are shown with components R_1, R_2, or R_3 in different colors. The component similar to that of the parent molecule is shown in black. (*A*) Six derivatives (B, D, E, F, H, and J) inhibited the aggregation of Aβ42. For each of these compounds, the time dependence of the reactive flux toward oligomers (*SI Appendix*, Eq. **S2**) for the aggregation of a 2 μM Aβ42 solution in the presence of either 1% DMSO (black) alone or with 2 μM (green), 6 μM (orange), or 10 μM (red) of the compound is shown; these reactive fluxes were estimated from the data shown in *SI Appendix*, Fig. S1 and literature (13). The OIC_{50}^{PT}, OIC_{25}^{T}, and KIC_{50}^{M} values determined from these reactive fluxes are shown for the positive compounds, i.e., with a significant effect on the aggregation kinetics. (*B*) Four other compounds (A, C, G, and I) did not affect the aggregation of Aβ42 significantly.

study (13)]. For four compounds (A, C, G, and I), no significant effects could be observed on the kinetics (*SI Appendix*, Fig. S1). For the remaining six compounds (B, D, E, F, H, and J), however, a progressive delay in the aggregation reaction could be observed in Aβ42 aggregation with increasing concentrations of the compounds (*SI Appendix*, Fig. S1). These six derivatives exhibited different effects on the $t_{1/2}$ of Aβ42 aggregation, each of which was estimated by determining its KIC_{50}^{M} value (*SI Appendix*, Fig. S2*A*).

We next carried out a semiempirical quantitative analysis of the effects of all seven positive compounds that inhibit Aβ42 aggregation by fitting the experimental aggregation profiles to a single rate law (19), thus obtaining the combined microscopic kinetic rate constants k_+k_n, which represent the overall rate constants of the primary pathways of aggregation, and k_+k_2, which represent the overall rate constants of the secondary pathways. These aggregation profiles in the presence of the inhibitors were then compared with the corresponding values evaluated in the absence of the compounds, to define the systematic perturbations of the microscopic combined rate constants in the rate law (see *Materials and Methods*). The results showed that the rates of both k_+k_n (primary pathways), and k_+k_2 (secondary pathways) were both decreased as a function of the concentration of small molecules (*SI Appendix*, Fig. S2 *B* and *C*).

To decouple the effects of the small molecules on the combined rate constants k_+k_n and k_+k_2, we carried out an additional set of experiments where Aβ42 aggregation in the presence of each molecule was monitored following the addition of 30% of preformed fibril seeds (*SI Appendix*, Fig. S3); under these conditions, the formation of amyloid fibrils is driven mainly by elongation processes (13). We observed that none of the molecules detectably affected the kinetics under these conditions at concentrations as high as 10 μM, indicating strongly that none affects significantly the rate of elongation of Aβ42 fibrils. Thus, the decrease in the combined rate constants obtained from the unseeded aggregation in the presence of the small molecules, k_nk_+ and k_2k_+, can be attributed solely to the decrease in k_n and k_2 (*SI Appendix*, Fig. S2).

A crucial aspect of the SKAR strategy is the analysis of the rate constants of the primary and secondary nucleation steps, which allows calculation of the reactive flux toward oligomers over time in the absence and presence of increasing concentrations of molecules (*Materials and Methods*, Fig. 2*A*, and *SI Appendix*, Fig. S4). Strikingly, the formation of Aβ42 oligomers over time was found to be both delayed and reduced by one or more of the set of all seven molecules discussed in the present study. The shift in the maximum reactive flux toward oligomers (OIC_{50}^{PT}, *SI Appendix*, Fig. S4*A*) and the total number of oligomers (OIC_{25}^{T}, *SI Appendix*, Fig. S4*B*) generated could be determined as a function of the concentration of each small molecule.

The values of KIC_{50}^{M}, OIC_{50}^{PT}, and OIC_{25}^{T} were then used to construct the KIA fingerprint for each compound to compare their potency in inhibiting macroscopic aggregation, delaying oligomer formation, and reducing the total number of oligomers formed (Fig. 3). The KIC_{50}^{M} values indicated that four molecules (J, F, D, and H) inhibited the overall rate of fibril formation in Aβ42 aggregation to a greater extent than the parent compound. In particular, molecule H, the most potent inhibitor, is three times more effective than its parent compound, bexarotene (Fig. 3).

Furthermore, a particularly important observation is that the same four molecules (J, F, D, and H) also showed an increased potency with respect to that of bexarotene in delaying the formation of oligomers (OIC_{50}^{PT}), and reducing the total number of oligomers over time (OIC_{25}^{T}) (Fig. 3). More specifically, molecule J exhibited the same potency as bexarotene in delaying the flux toward oligomers, but exhibited an increased potency in reducing the total number of oligomers formed. On the other hand, molecule E, which is less potent than bexarotene in inhibiting the aggregation kinetics and delaying the flux toward oligomers, was slightly more effective than bexarotene in reducing the total number of oligomers generated during the reaction.

Establishment of the SKAR Rules: Identification of the Physicochemical Parameters That Lead to an Increased Potency in Reducing Oligomer Production. Taken together, the effects described in this study provide an opportunity to identify chemical features that could account for the potency of the molecules in inhibiting the aggregation of Aβ42. They indicate, in particular, that the combination of polar and apolar (R_1 and R_3) components is essential for the activity of the parent molecule. Thus, neither molecule A nor molecule I, both of which lack the carboxylic acid group present in bexarotene, affects the aggregation of Aβ42 (Fig. 2*B* and *SI Appendix*, Fig. S1), suggesting that a polar moiety containing an acidic ionizable group is essential for inhibitory activity. In addition, molecule C, which lacks the cyclohexane group of bexarotene, is inactive, suggesting that the apolar nature of the component R_3 is also crucial for an inhibition of the aggregation process. Furthermore, although compound F, where the linker group is modified, is still able to inhibit the aggregation of Aβ42, compound G, which contains an additional polar carbonyl group in the apolar component (R_3) compared with molecule F, no longer has activity. These findings suggest that essential apolar interactions are made between the R_3 moiety of the molecule and Aβ42, such that modifications to include a polar group would eliminate this interaction.

On the basis of these results, we generated a specific pharmacophore based on the chemical structures of all of the bexarotene derivatives found to possess inhibitory activity (*SI Appendix*, Fig. S5) (25–28). The features of this pharmacophore are fully consistent with the findings discussed above, including the conclusion that the detailed nature of the linker is not essential for inhibiting Aβ42 aggregation, while the apolar and polar groups play key roles in this process.

In particular, all compounds with an altered linker component (B, D, E, F, and H) but that preserve the nature of the polar R_1 and apolar R_3 moieties of bexarotene were effective in inhibiting the aggregation of Aβ42. Minor modifications to the linker group are thus possible without losing activity. In addition, analysis of the physicochemical properties of the linker components (*SI Appendix*, Table S2) did not reveal any correlation between the potency of the compound and the overall polarity, length, or flexibility of the linker region (29). These results suggest that the R_2 component is not responsible for forging any critical interactions required for the inhibition of Aβ42 aggregation. We therefore infer that the linker is primarily responsible for

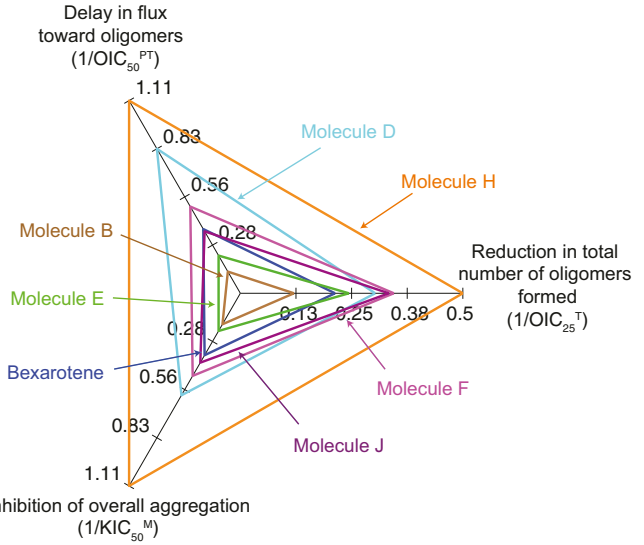

Fig. 3. KIA fingerprint of the bexarotene scaffold. KIA fingerprints are shown for bexarotene and its positive derivatives (represented by different colors) to compare their potencies.

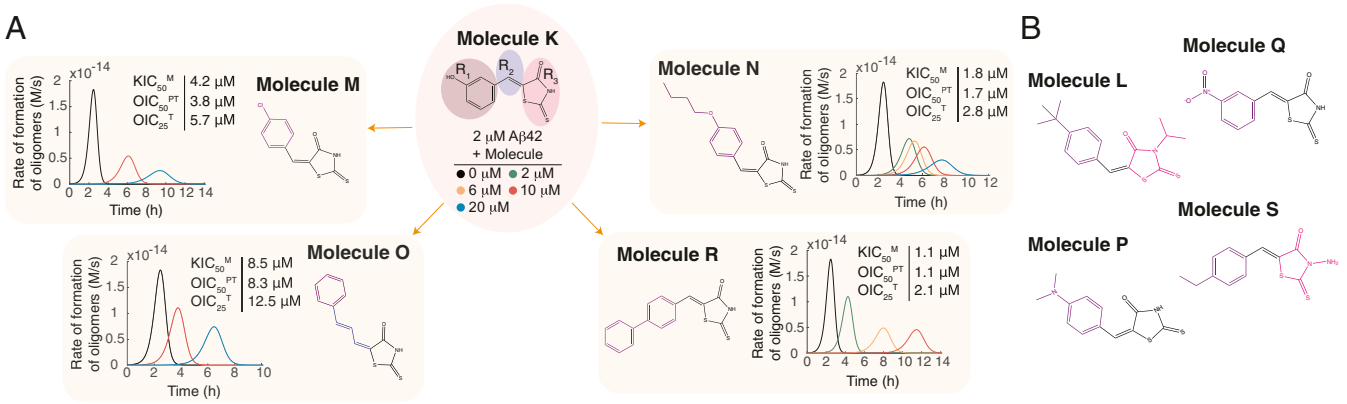

Fig. 4. Application of the SKAR rules to the development of a rhodanine-based active compound. The eight derivatives of the rhodanine-based compound K (L through S) used in this study are shown with components R_1, R_2, or R_3 in different colors. The component that is similar to that of the parent molecule is shown in black. (*A*) Four compounds (M, N, O, and R) inhibited the aggregation of Aβ42. For each of these compounds, the time dependence of the reactive flux toward oligomers (*SI Appendix*, Eq. **S2**) for the aggregation of a 2 μM Aβ42 solution in the presence of either 1% DMSO alone (black) or with 2 μM (green), 6 μM (orange), 10 μM (red), or 20 μM (blue) of the compound is shown; these reactive fluxes were estimated from the data shown in *SI Appendix*, Fig. S6. The OIC_{50}^{PT}, OIC_{25}^{T}, and KIC_{50}^{M} values determined from these reactive fluxes are shown for the positive compounds. (*B*) Four other compounds (L, P, Q, and S) did not affect the aggregation of Aβ42 significantly.

orientating the polar and apolar components in the optimal positions. This conclusion is also consistent with our pharmacophore model (*SI Appendix*, Fig. S5). We do note, however, that molecules F and J have a longer linker length compared with bexarotene. This greater distance, which could allow a higher degree of flexibility of binding for components R_1 and R_3, could account for the higher inhibitory potency observed in molecules F and J compared with bexarotene (*SI Appendix*, Table S2).

As we compared the apolarity of the R_3 component between bexarotene and molecules E and H, we found that the apolarity of the R_3 component is correlated with the potency of the associated scaffold (*SI Appendix*, Table S3) (30). In particular, when comparing molecules H and F, we found that an extended apolar structure results in an overall more pronounced KIA fingerprint.

Implementation of the SKAR Rules: Generation of Active Derivatives from an Inactive Parent Compound. To illustrate how the SKAR rules derived above could be applied in a rational drug discovery program directed toward AD, we applied them to a scaffold different from that of bexarotene, which contains a central rhodanine functional group. Rhodanine-based compounds are frequently used in medicinal chemistry, since they are well tolerated and exhibit a variety of pharmacological activities (31). In particular, rhodanine-based compounds have been found to inhibit the aggregation of tau, and thus have been suggested, in a different context, as potential drugs against AD (31). The central molecule of the present SKAR procedure is molecule K, which has three chemical components: polar R_1 and R_3 components and an R_2 linker component. When we monitored the aggregation of a 2-μM sample of Aβ42 in the presence of the parent molecule K, no effect of the compound could be observed (Fig. 4*A* and *SI Appendix*, Fig. S6).

Molecule K, however, lacks the dual polar–apolar nature of the R_1 and R_3 moieties in the pharmacophore, which, in the study of the bexarotene derivatives discussed above, was judged as essential for the activity of the compound. We therefore studied the effects of a set of derivatives of molecule K (M, N, O, and R), which we modified to include such polar and apolar components, on the aggregation kinetics of Aβ42 with a concentration range between 2 μM and 20 μM. As expected from the conclusions above, all four compounds were found to inhibit the aggregation of Aβ42; further studies showed that this inhibition showed a clear concentration dependence (Fig. 4*A* and *SI Appendix*, Fig. S6).

As negative controls, we considered molecules P and Q, in which, like the parent molecule K, both R_1 and R_3 moieties are polar, and neither was found to have a detectable effect on the aggregation of Aβ42. As a further negative control, molecule L, which possesses an apolar R_3 moiety but an R_1 component of lower polarity than in compound K, again showed no significant effect on Aβ42 aggregation, thus further supporting the importance of the dual apolar–polar character of the pharmacophore. Along similar lines, molecules M, N, O, and R showed no effect on Aβ42 aggregation under seeding conditions (*SI Appendix*, Fig. S7), indicating that the elongation process of Aβ42 was not affected by these molecules.

Since extending the apolar nature of the aggregation inhibitors discussed above was found to increase their potency, we sought to assess whether or not extending the polar nature could have a similar effect on the compounds based on molecule K. We therefore studied Aβ42 aggregation in the presence of molecule S, in which a primary amine extension is added. We found that the activity of the molecule was essentially abolished (Fig. 4*B*

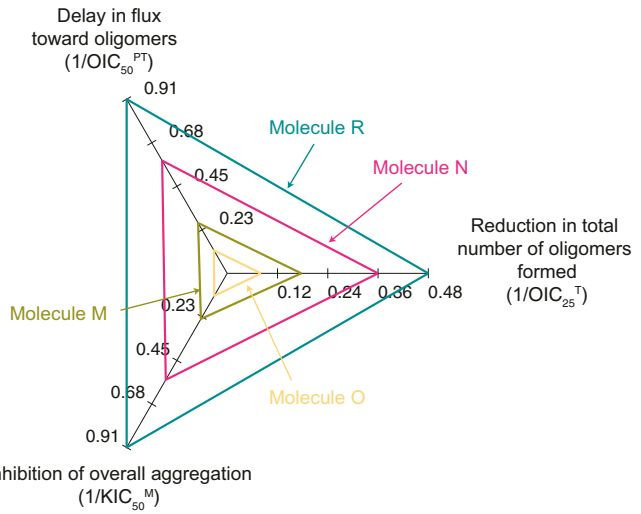

Fig. 5. KIA fingerprint of the rhodanine-based compounds. KIA fingerprints are shown for the positive rhodanine-based compounds (represented by different colors) to compare their potencies.

and *SI Appendix*, Fig. S6 and Table S4) (30), although we note that this lack of activity might be also be due to the fact that the R_1 component was not apolar enough.

As observed for bexarotene, these results indicate that an extended apolar nature leads to a higher potency of the molecule in inhibiting Aβ42 aggregation. Indeed, molecules N and R, which both have extended apolar components compared with the positive molecule O (with R having the most apolar component), are able to delay oligomer formation, as well as inhibit more effectively the overall oligomer production (Fig. 4 and *SI Appendix*, Fig. S8 and Table S5) (30). The KIA fingerprints of the positive molecules were generated as previously (*SI Appendix*, Fig. S8) and showed that the molecules inhibit the aggregation kinetics of Aβ42 with overall potencies in the order R > N > M > O (Fig. 5).

Discussion

In SAR studies, the availability of robust preclinical primary assays has enabled traditional drug discovery programs to be highly successful in identifying potent inhibitors of specific disease-associated proteins, in particular for enzymes and signaling receptors. In these assays, dose–response binding curves can be obtained with high reproducibility, thus giving a detailed understanding of the mechanism of action of the inhibitor, as well as a quantitative means of assessing the relative potency of potential drugs, such as IC_{50} values. In the case of protein aggregation, however, such assays have been difficult to develop because of a range of technical challenges, including the fact that many of the proteins involved are not natively folded and their aggregation behavior is dominated by complex kinetic factors rather than thermodynamic ones (12, 15). As such, beyond a generic description of a delay or reduction in the rate of formation of fibrils, current approaches provide only very limited information about the rates of change of other species in the aggregation reaction, including, in particular, oligomers.

This situation is now changing with the development of methods for dissecting the protein aggregation process into its microscopic steps, making it possible to target the specific pathways that give rise to pathogenic agents, notably the relatively small oligomeric species that are commonly observed as intermediates in the process of aggregation. By analogy with conventional SAR approaches, where IC_{50} values are used to address the specificity of small molecules to targets, the SKAR platform that we have described here defines quantitative parameters, such as OIC_{50}^{PT} and OIC_{25}^{T}, which describe the efficacy of such molecules in inhibiting specifically the formation of potentially pathogenic oligomeric species. SKAR, therefore, tackles the limitations of current SAR approaches used to identify potential protein aggregation inhibitors by specifically addressing the effect of these small molecules in suppressing oligomer population, rather than their effects on the complete aggregation process itself. Therefore, our approach complements conventional SAR drug discovery techniques designed to measure binding affinities with kinetics-based tools to target neurodegenerative diseases.

We observe that effective therapeutic approaches for such diseases may have the goal of providing additional capacity to our natural protective systems, which, as we age, become slowly but progressively impaired. In this view, identifying compounds that cause even relatively small but significant changes in the production of oligomeric species, such as those demonstrated here, could extend the period of cognitive health.

Materials and Methods

Recombinant Aβ42 was expressed in *Escherichia coli*, as described (21). Aggregation experiments were performed using a ThT fluorescence assay as described (18, 19). Kinetic rate constants were obtained using a kinetic analysis as described (18, 19).

Full methods are available in *SI Appendix, Materials and Methods*.

ACKNOWLEDGMENTS. We thank Dr. Kerry Jenkins for useful discussions. We acknowledge support from the Centre for Misfolding Diseases (S.C., J.H., T.C.T.M., T.P.J.K., C.M.D., and M.V.); the Agency for Science, Technology, and Research, Singapore (S.C.); Peterhouse College, Cambridge (T.C.T.M.); the Swiss National Science Foundation (T.C.T.M.); the Knut & Alice Wallenberg Foundation (S.L.); the European Research Council (S.L.); the Swedish Research Council (S.L.); the Frances and Augustus Newman Foundation (T.P.J.K.); the UK Biotechnology and Biochemical Sciences Research Council (C.M.D. and M.V.); and the Wellcome Trust (C.M.D., T.P.J.K., and M.V.).

1. Alzheimer's Association (2014) 2014 Alzheimer's disease facts and figures. *Alzheimers Dement* 10:e47–e92.
2. Knowles TPJ, Vendruscolo M, Dobson CM (2014) The amyloid state and its association with protein misfolding diseases. *Nat Rev Mol Cell Biol* 15:384–396.
3. Selkoe DJ, Hardy J (2016) The amyloid hypothesis of Alzheimer's disease at 25 years. *EMBO Mol Med* 8:595–608.
4. De Strooper B, Karran E (2016) The cellular phase of Alzheimer's disease. *Cell* 164: 603–615.
5. Eisenberg D, Jucker M (2012) The amyloid state of proteins in human diseases. *Cell* 148:1188–1203.
6. Holtzman DM, Morris JC, Goate AM (2011) Alzheimer's disease: The challenge of the second century. *Sci Transl Med* 3:77sr1.
7. Bieschke J, et al. (2011) Small-molecule conversion of toxic oligomers to nontoxic β-sheet-rich amyloid fibrils. *Nat Chem Biol* 8:93–101.
8. Karran E, Hardy J (2014) A critique of the drug discovery and phase 3 clinical programs targeting the amyloid hypothesis for Alzheimer disease. *Ann Neurol* 76:185–205.
9. Aguzzi A, O'Connor T (2010) Protein aggregation diseases: Pathogenicity and therapeutic perspectives. *Nat Rev Drug Discov* 9:237–248.
10. Golde TE, Schneider LS, Koo EH (2011) Anti-aβ therapeutics in Alzheimer's disease: The need for a paradigm shift. *Neuron* 69:203–213.
11. Hamrang Z, Rattray NJW, Pluen A (2013) Proteins behaving badly: Emerging technologies in profiling biopharmaceutical aggregation. *Trends Biotechnol* 31:448–458.
12. Arosio P, Vendruscolo M, Dobson CM, Knowles TPJ (2014) Chemical kinetics for drug discovery to combat protein aggregation diseases. *Trends Pharmacol Sci* 35:127–135.
13. Habchi J, et al. (2017) Systematic development of small molecules to inhibit specific microscopic steps of Aβ42 aggregation in Alzheimer's disease. *Proc Natl Acad Sci USA* 114:E200–E208.
14. Haass C, Selkoe DJ (2007) Soluble protein oligomers in neurodegeneration: Lessons from the Alzheimer's amyloid beta-peptide. *Nat Rev Mol Cell Biol* 8:101–112.
15. Young LM, Ashcroft AE, Radford SE (2017) Small molecule probes of protein aggregation. *Curr Opin Chem Biol* 39:90–99.
16. Fusco G, et al. (2017) Structural basis of membrane disruption and cellular toxicity by α-synuclein oligomers. *Science* 358:1440–1443.
17. Flagmeier P, et al. (2017) Ultrasensitive measurement of Ca^{2+} influx into lipid vesicles induced by protein aggregates. *Angew Chem Int Ed Engl* 56:7750–7754.
18. Knowles TPJ, et al. (2009) An analytical solution to the kinetics of breakable filament assembly. *Science* 326:1533–1537.
19. Cohen SIA, et al. (2013) Proliferation of amyloid-β42 aggregates occurs through a secondary nucleation mechanism. *Proc Natl Acad Sci USA* 110:9758–9763.
20. Cohen SIA, et al. (2015) A molecular chaperone breaks the catalytic cycle that generates toxic Aβ oligomers. *Nat Struct Mol Biol* 22:207–213.
21. Habchi J, et al. (2016) An anticancer drug suppresses the primary nucleation reaction that initiates the production of the toxic Aβ42 aggregates linked with Alzheimer's disease. *Sci Adv* 2:e1501244.
22. Arosio P, et al. (2016) Kinetic analysis reveals the diversity of microscopic mechanisms through which molecular chaperones suppress amyloid formation. *Nat Commun* 7: 10948.
23. Hellstrand E, Boland B, Walsh DM, Linse S (2010) Amyloid β-protein aggregation produces highly reproducible kinetic data and occurs by a two-phase process. *ACS Chem Neurosci* 1:13–18.
24. Michaels TCT, Lazell HW, Arosio P, Knowles TPJ (2015) Dynamics of protein aggregation and oligomer formation governed by secondary nucleation. *J Chem Phys* 143: 054901.
25. Sadowski J, Gasteiger J, Klebe G (1994) Comparison of automatic three-dimensional model builders using 639 X-ray structures. *J Chem Inf Model* 34:1000–1008.
26. Schneidman-Duhovny D, Dror O, Inbar Y, Nussinov R, Wolfson HJ (2008) PharmaGist: A webserver for ligand-based pharmacophore detection. *Nucleic Acids Res* 36: W223–W228.
27. OpenEye Scientific Software (2017) ROCS 3.2.2.2. Available at http://www.eyesopen.com. Accessed September 24, 2017.
28. Hawkins PCD, Skillman AG, Nicholls A (2007) Comparison of shape-matching and docking as virtual screening tools. *J Med Chem* 50:74–82.
29. Haynes WM (2014) *CRC Handbook of Chemistry and Physics* (CRC, Boca Raton, FL).
30. Tetko IV, et al. (2005) Virtual computational chemistry laboratory–Design and description. *J Comput Aided Mol Des* 19:453–463.
31. Bulic B, et al. (2009) Development of tau aggregation inhibitors for Alzheimer's disease. *Angew Chem Int Ed Engl* 48:1740–1752.